


Article

Spatio-Temporal Diversity in the Link between Tree Radial Growth and Remote Sensing Vegetation Index of Qinghai Spruce on the Northeastern Margin of the Tibetan Plateau

Mengyuan Wei ^{1,2}, Liang Jiao ^{1,2,*} , Peng Zhang ^{1,2}, Xuan Wu ^{1,2}, Ruhong Xue ^{1,2} and Dashi Du ^{1,2}

¹ College of Geography and Environment Science, Northwest Normal University, No.967, Anning East Road, Lanzhou 730070, China

² Key Laboratory of Resource Environment and Sustainable Development of Oasis, Northwest Normal University, Lanzhou 730070, China

* Correspondence: jiaoliang@nwnu.edu.cn; Tel.: +86-139-1935-0195

Abstract: Global warming is causing some regions to experience frequent and severe drought, with important impacts on montane forest vegetation. In this study, the Qilian Mountains is on the northeastern margin of the Tibetan Plateau which was divided into three study areas, the eastern (HaXi), middle (XiShui) and western (QiFeng) parts. This work focused on interannual trend comparison of tree-ring width (TRW) and enhanced vegetation index (EVI), their relationship characterization from 2000 to 2020, and spatial and temporal pattern portrayal of response to climate factors. The results showed that: (1) the overall interannual variation of TRW and EVI showed a stable increasing trend, and the trend of TRW and EVI gradually became consistent with the increase in drought stress (from the eastern region to the western region and from high elevation to low elevation) ($p < 0.01$); (2) a significant positive relation was observed between TRW and EVI at the same sampling sites, and the synchrony of the positive correlation gradually increased with the increase of drought stress ($p < 0.01$); and (3) compared to TRW, EVI is significantly more sensitive with climatic variations, and the dominant climate factors affecting both TRW and EVI dynamics are gradually identical with the increase of drought stress.

Keywords: global climate change; northeastern Tibetan Plateau; enhanced vegetation index; tree-ring width; Qinghai spruce (*Picea crassifolia* Kom.)



Citation: Wei, M.; Jiao, L.; Zhang, P.; Wu, X.; Xue, R.; Du, D. Spatio-Temporal Diversity in the Link between Tree Radial Growth and Remote Sensing Vegetation Index of Qinghai Spruce on the Northeastern Margin of the Tibetan Plateau. *Forests* **2023**, *14*, 260. <https://doi.org/10.3390/f14020260>

Academic Editor: Giovanni Leonelli

Received: 15 December 2022

Revised: 25 January 2023

Accepted: 28 January 2023

Published: 30 January 2023



Copyright: © 2023 by the authors. Licensee MDPI, Basel, Switzerland. This article is an open access article distributed under the terms and conditions of the Creative Commons Attribution (CC BY) license (<https://creativecommons.org/licenses/by/4.0/>).

1. Introduction

The Intergovernmental panel on climate change (IPCC) Sixth Assessment Report [1] highlighted that even if global warming levels stabilize at 1.5 °C to 2.0 °C, some regions will still experience more frequent and severe ecological drought [2]. As global temperature increases, forest cover, carbon and nitrogen cycles, and ecosystem boundaries in the Mediterranean basin and arid and semi-arid regions of Asia are strongly affected. Climate change can directly affect tree growth, phenology, and resource allocation. Thus, it has important impacts on forest production, forest community structure, carbon stocks and species composition [3,4]. Both tree-ring width (TRW) and satellite remote sensing monitoring data indicate that global warming is already causing significant changes in xylem growth and aboveground primary productivity in many boreal and tundra ecosystems, and has already led to more frequent and widespread events that may cause significant negative influences on forest productivity as well as tree growth, and will lead to forest dieback and tree mortality [5–10]. However, in some places, it has been observed that warming has accelerated the rate of tree growth and increased forest biomass. [11–13]. Therefore, it is uncertain whether the climate change will have a huge impact on forest ecosystems; it is important to study the linkages between forest productivity and tree growth and how forest productivity and tree growth respond to climate change.

Both TRW and vegetation index are widely used in forest management and ecological research. TRW can determine the amount of wood formed by stems, which is closely related to biomass increase and carbon sequestration capacity, and TRW is also an important indicator of climate change [14,15]. Vegetation index, which is acquired through satellite remote sensing platforms, is an indicator of vegetation condition obtained by using differences in vegetation absorption and reflection spectra at different wavelengths and can be used to characterize changes in tree primary productivity across spatial scales as well as to assess variations in interannual tree growth and carbon stock. Most previous studies have analyzed the link between TRW and vegetation indices, but obtained different results. A global-scale study of the relationship between vegetation index and tree growth, categorizing different forest types and regional climates into eight patterns, found that TRW and vegetation index were closely coupled on an annual scale and that there was an overall positive correlation between them [16]. Another study in the Sierra Nevada showed a significant relationship between vegetation index and TRW with a five-month lag, and within each individual site, the interannual correspondence between gross primary productivity with a legacy effect and tree growth was stronger [17]. Studies in northwestern Russia, Siberia and other regions indicate that vegetation index is affiliated with TRW [18–21]. However, studies in North America, subarctic mountains, and high altitudes in Russia and Canada have demonstrated that there is no relationship between vegetation index and TRW [22–24]. Both TRW and vegetation index can characterize tree growth, and some studies have shown that TRW and the vegetation index respond to climate change in a consistent manner [25,26]. However, a study which used the Vaganov–Shashkin Lite model to derive xylem phenology showed that the dominant climate factors for TRW and vegetation index are consistent in North America and temperate grassland regions [27], but they are inconsistent in the Mediterranean and central Europe. There are no clear results on the association among vegetation index, TRW and climate factors. Combining TRW with accurate enhanced vegetation index (EVI) data can provide a united assessment of leaf and stem growth, which could help solve the problem of forest productivity.

Northwest China, as an important treasure trove of forest resources, has forest ecosystems that are very sensitive to climate change response. The Qilian Mountains are located at the northeastern edge of the Tibetan Plateau in the arid and semi-arid transition zone of northwestern China. As an important mountain range in northwestern China, glacier melting, climate change and vegetation variations will significantly influence the oasis for farming in China's 'Belt and Road' region. Qinghai spruce (*Picea crassifolia* Kom.) is a dominant tree species in the Qilian Mountains that occupies about 20.5% of the forest area and plays a considerable role in regulating climate, containing water, and combating desertification [28]; it is an important ecological security barrier in western China. Currently, a majority of studies have used TRW for climate reconstruction and changes in TRW and vegetation index under climate change conditions in the Qilian Mountains, while the coupling between EVI and TRW as well as comparative study of their sensitivity to climate are still limited. Our study fills the lack of exploring the interconnection among EVI, TRW and climate change and their spatial and temporal patterns on the northeastern edge of the Tibetan Plateau. Drought stress in the Qilian Mountains has been gradually decreasing during the last two decades [29]; thus, a more in-depth study of the connection between forest productivity and radial growth of trees in the Qilian Mountains and their linkage to climate change is crucial for ecological conservation in the region, as well as for the sustainable use of forest resources in northwest China.

In this study, based on the context of global warming, we combined annual tree-ring data collected from the eastern, central, and western Qilian Mountains with remote sensing data to investigate the link between EVI, tree radial growth, and climate change. Our goals were: (1) to compare and analyze trends in changes in TRW and EVI and their spatial and temporal patterns in the Qilian Mountains; (2) to quantify the relationship between TRW and EVI and their spatial and temporal patterns in the Qilian Mountains; and (3)

to analyze the consistency of factors which affect the activity of tree radial growth and vegetation canopy.

2. Data and Methods

2.1. Study Sites

The Qilian Mountains are located on the northeastern edge of the Tibetan Plateau (Figure 1), with a length of about 800 km and a width of about 200–400 km and are distributed in a northwest–southeast trending belt. The highest elevation of the Qilian Mountains is 5808 m and they rise gradually from southeast to northwest. The climate of the study area is temperate continental. As one of the dominant species in the study area, Qinghai spruce is a hardy and shade-tolerant species with high canopy closure and few understory shrubs, usually growing on shady and semi-shady slopes at elevations of 2500–3400 m a.s.l [30].

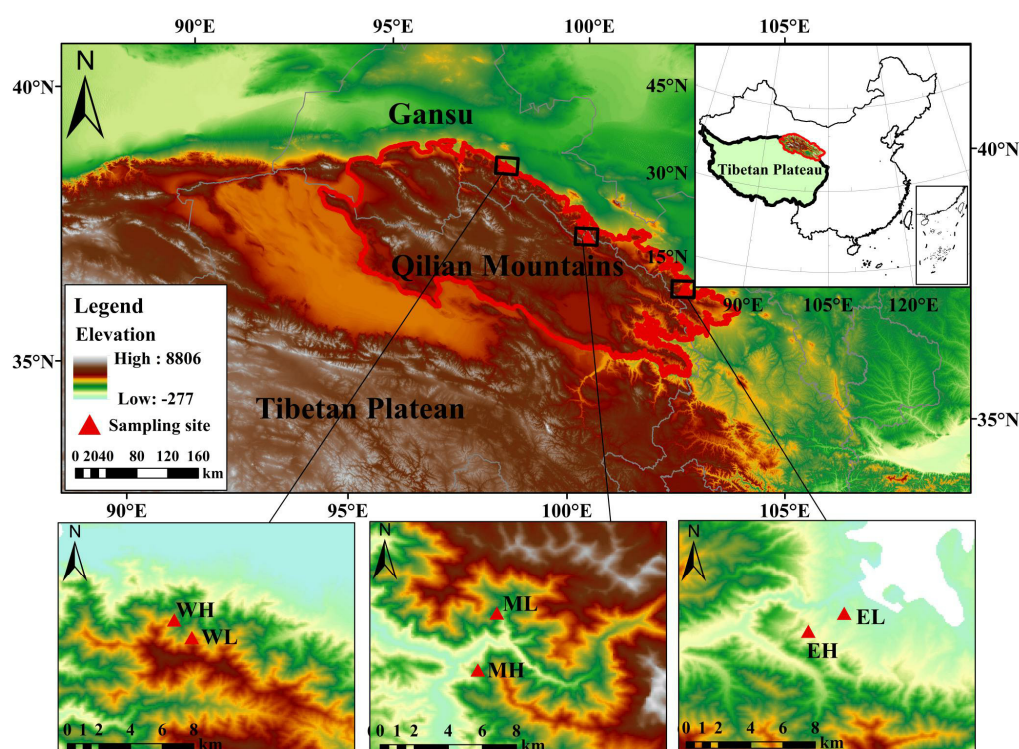


Figure 1. Study regions and distribution of sampling sites at different elevations.

We selected two different elevations as sampling sites in the eastern, middle, and western regions of the Qilian Mountains, and named them as eastern high elevation (EH), eastern low elevation (EL), middle high elevation (MH), middle low elevation (ML), western high elevation (WH), and western low elevation (WL), sequentially (Figure 1).

According to meteorological data, the monthly maximum values of both precipitation and temperature factors were concentrated from May to September, which is also the growing season of Qinghai spruce (Figure 2).

The total annual precipitation in the eastern region of the Qilian Mountains was 292 mm. In the central region, the total annual precipitation was 189 mm and in the western region, the total annual precipitation was 106 mm (Figure 3).

Combined with relevant studies and meteorological data, the eastern region of the Qilian Mountains has the most moisture and the environment of the Qilian Mountains becomes increasingly arid from east to west [31,32].

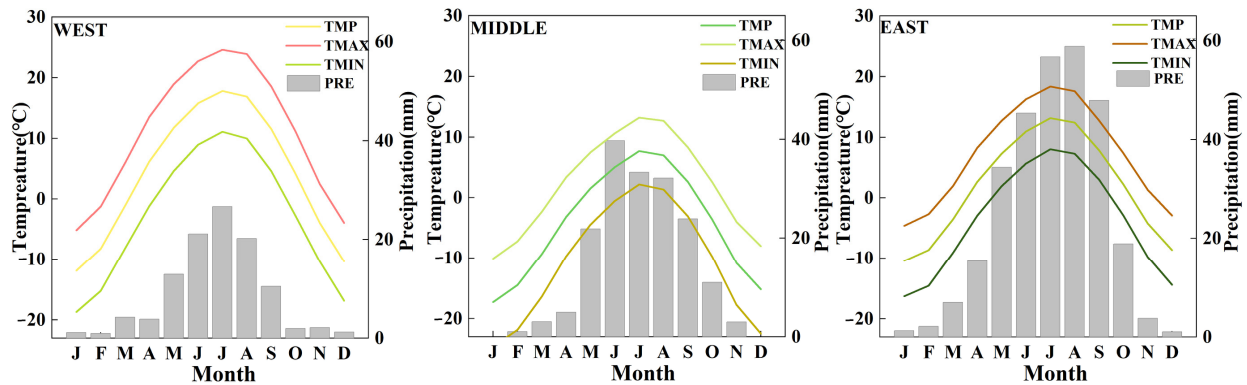


Figure 2. Monthly variability of the mean minimum temperature (TMN), mean temperature (TMP), mean maximum temperature (TMAX) and total precipitation (PRE) from 1960 to 2020.

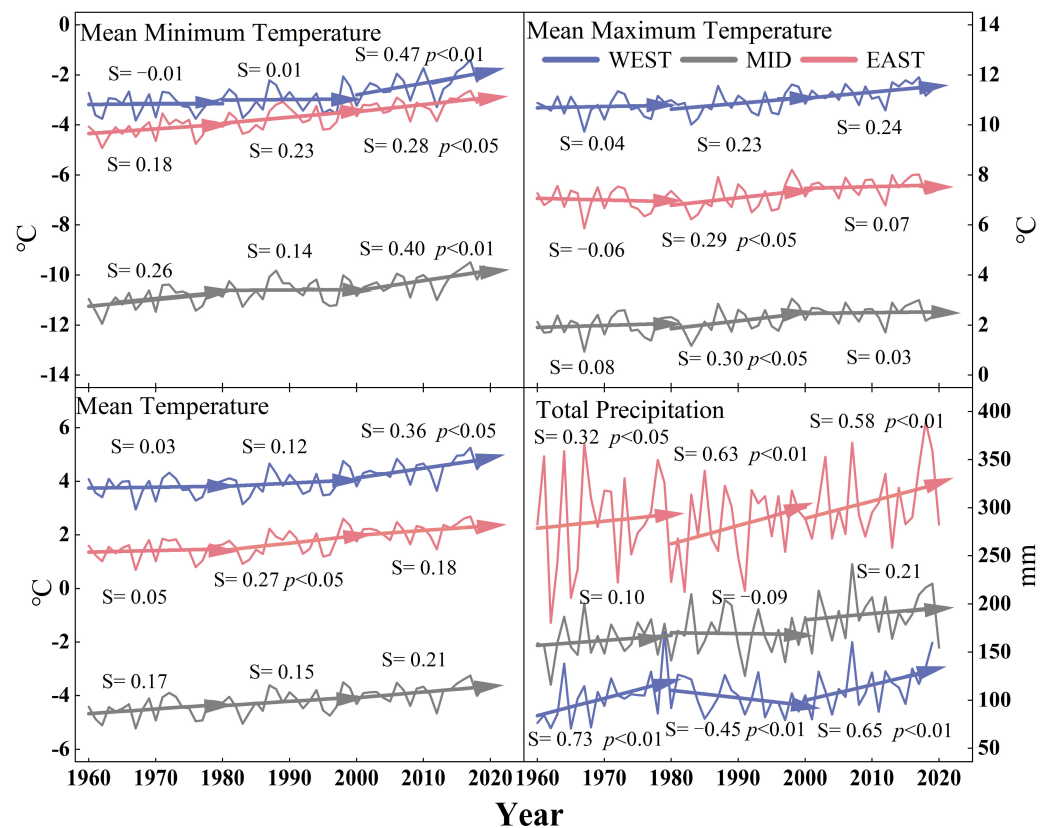


Figure 3. Interannual variability of the mean maximum temperature, mean temperature, mean minimum temperature, and total precipitation from 1960 to 2020 in three regions of the Qilian Mountains from east to west (s—slope; solid line with arrows—linear regression).

2.2. Tree-Ring Data

We selected an area with little anthropogenic disturbance in the Qilian Mountains to conduct sampling of Qinghai spruce in 2021. The elevations of these sampling plots ranged from 2574 m a.s.l to 3305 m a.s.l (Table 1).

To obtain more accurate and valid TRW data in cross-dating, we selected 25 healthy trees undisturbed by fire, disease, and pests and without significant physical damage as samples at each sampling plot. We used a 5.15 mm increment borer to extract two sample cores from each tree at a DBH of 1.3 m along the mountain in different directions. Finally, 150 trees of Qinghai spruce were sampled, with a total of 300 tree-ring cores.

Table 1. Information about the sampling sites of Qinghai spruce.

Region	Western Region		Middle Region		Eastern Region	
Site	WH	WL	MH	ML	EH	EL
Elevation (m a.s.l.)	3070	2650	3300	2585	3025	2574
Latitude (N)	39.55	39.54	38.32	38.35	37.40	37.41
Longitude (E)	98.08	98.09	100.18	100.19	102.54	102.56
Slope	35°	23°	30°	19°	41°	31°
CC (%)	32%	38%	40%	45%	50%	55%
TD (m)	4.60	5.20	6.00	7.20	5.30	6.80
DBH (cm)	31.00	38.00	40.00	31.10	32.20	32.20
TH (m)	11.00	13.00	20.30	16.30	18.00	16.50

CC—canopy coverage; TD—tree distance; DBH—diameter at breast height; TH—tree height.

All collected samples were brought back to the laboratory, and later the tree-ring cores were polished with different sizes of sandpaper until the rings were clearly visible, after which the cores were initially cross-dated under a microscope to determine the widths of the tree rings, missing rings and false rings, so that the years of the two cores from each tree corresponded accurately. LINTAB6 and COFECHA with an accuracy of 0.001 mm were used to measure the tree-ring width and cross-date the sample cores in sequence [33].

When building the chronology, the ARSTAN program was used to remove the trees' own growth trends and calculate the chronology of the tree rings. The chronology with the trends removed can excise the influence of non-climatic factors on radial growth and make the chronology more reliable [34]. Ultimately, we obtained six standardized chronologies of Qinghai spruce tree-ring width and counted the characteristic parameters of the chronology (Table 2). MS is a statistic that measures year-to-year changes in tree-ring width. The SD reflects the interannual variability of each chronology. AC1 represents the effect of the previous year's climate on the current year's growth. PC1 indicates the percentage of variance explained by the first component in a principal component analysis. R reflects the common signal strength among chronologies. SNR and EPS represent the intensity of the common climate information between chronologies, and a chronology was used for dendroclimatological analysis with $EPS > 0.85$ (Table 2).

Table 2. Dendrochronological characteristics of chronologies for the Qinghai spruce.

Region	Western Region		Middle Region		Eastern Region	
Site	WH	WL	MH	ML	EH	EL
Core/tree	50/25	50/25	50/25	50/25	50/25	50/25
Time period	1934–2020	1947–2020	1951–2020	1937–2020	1951–2020	1937–2020
Mean age	74	65	52	66	52	70
MS (mean sensitivity)	0.179	0.330	0.224	0.307	0.108	0.222
SD (standard deviation)	0.243	0.293	0.220	0.326	0.146	0.244
AC1 (first-order serial autocorrelation)	0.610	0.174	0.637	0.479	0.146	0.439
R (mean correlation of all series)	0.442	0.579	0.258	0.671	0.312	0.416
R1 (mean correlation within-trees)	0.576	0.843	0.475	0.843	0.377	
R2 (mean correlation between-trees)	0.438	0.594	0.253	0.660	0.215	0.402
PC1 (first principal component)	0.486	0.638	0.303	0.703	0.369	0.454
SNR (signal-to-noise ratio)	32.51	25.221	23.259	63.084	7.268	15.694
EPS (expressed population signal)	0.970	0.962	0.959	0.984	0.879	0.940

2.3. EVI Data

The EVI data for this study were obtained from the MOD13A2 product issued by NASA ("<https://www.nasa.gov/>" (accessed on 5 December 2021)), 16-day synthetic data with a spatial resolution of 1 km and projection of Albers conical equal-area. All study areas were pre-processed using the quality flags supplied by MODIS vegetation index products. Based on these quality flags, all images with clouds, cloud shadows, water, snow, ice and high levels of aerosols were eliminated from the pixels. Then we used MRT software to

batch stitch and crop, extract the specified band, and output the raster image. Ultimately, in order to further eliminate the interference of clouds, atmosphere, and solar altitude angle, the annual maximum EVI time series from 2000 to 2020 were then calculated using the international maximum value composites (MVC) method.

2.4. Meteorological Data

This work used several climatic data to investigate the relationship between climate, tree growth and vegetation canopy activity. In this study, meteorological data came from the Royal Netherlands Meteorological Institute ("<http://climexp.knmi.nl/>" (accessed on 13 December 2021)). Meteorological data were extracted from the CRUTS4.04 climate data grid from 1960 to 2020 with a spatial resolution of $0.5^\circ \times 0.5^\circ$. The grid data are spatially continuous average data obtained by a spatial interpolation technique using discrete meteorological station data, and the grid data have a certain spatial representativeness. Moreover, the meteorological stations belonging to the sampling sites are almost all in the city, which better reflects the meteorological changes of a city rather than the sampling sites. Therefore, the grid data are more representative of the actual situation of the sampling sites. The extracted climate data include monthly mean maximum temperature, monthly mean temperature, monthly mean minimum temperature, precipitation, and vapor pressure deficit (VPD). The standardized precipitation evapotranspiration index (SPEI) on a three-month time scale was used in this study, and the SPEI data were obtained from ("<http://sac.csic.es/spei/database.html>" (accessed on 9 May 2022)). There is a "Lag effect" in tree physiology, so we selected climatic factors from September of the previous year to October of the current year to correlate with TRW and EVI, respectively.

2.5. Statistical Analysis

2.5.1. Gleichläufigkeit (GLK) Index for the Six Chronologies

We calculated the GLK index for the six interannual chronologies to show inter-correlation between chronologies. From east to west, the GLK index between the two chronologies gradually increased (Table 3). The percentage of GLK represents the consistency of two chronological curves at a very high frequency, and a high GLK value represents similarity in growth patterns and factors limiting growth [35]. For a given year, table x , there exists an amount of variation between the adjacent two years i and $i + 1$. At this point, define $\Delta i > 0$, $G_{ix} = 1/2$; if $\Delta i = 0$, $G_{ix} = 0$; if $\Delta i < 0$, $G_{ix} = -1/2$. The GLK was calculated as:

$$GLK_{x,y} = \frac{1}{n-1} \sum_{i=1}^{n-1} |G_{ix} + G_{iy}|. \quad (1)$$

Table 3. GLK between the six chronologies (1960–2020).

	WH	WL	MH	ML	EH	EL
WH	100%	79.5% ***	63.1% *	58.1%	55.7%	50.8%
WL		100%	54.0%	67.2% **	45.0%	58.1%
MH			100%	52.4%	54.9%	50.0%
ML				100%	53.2%	58.1%
EH					100%	54.0%
EL						100%

*** $p < 0.001$; ** $p < 0.01$; * $p < 0.05$.

If $50 + \frac{(1.654 \times 50)}{\sqrt{n}} < GLK < 50 + \frac{(2.236 \times 50)}{\sqrt{n}}$, the correlation coefficients have significant change at 0.05 level; if $50 + \frac{(2.236 \times 50)}{\sqrt{n}} < GLK < 50 + \frac{(3.090 \times 50)}{\sqrt{n}}$, the correlation coefficients have significant change at 0.01 level; if $GLK > 50 + \frac{(3.090 \times 50)}{\sqrt{n}}$, the correlation coefficients have significant change at 0.001 level. n represents the number of samples in the two chronologies.

2.5.2. Theil–Sen Median and Mann–Kendall Test

Theil–Sen was used to analyze the trends of EVI from 2000 to 2020 on an image-by-image basis. The calculation equation is as follows [36,37]:

$$Seen_{slope} = median\left(\frac{x_j - x_i}{j - i}\right), \quad 1 < i < j < n, \quad (2)$$

where $Seen_{slope}$ represents the value of Sen' slop, and x_i and x_j represent the value of the variable at i time and j time, respectively. When $Seen_{slope} > 0$, it indicates that the time series is on the rise, and when $Seen_{slope} < 0$, it indicates that the time series is on the decrease.

Similarly, the Mann–Kendall test has similar merits to the Theil–Sen slope in that it effectively avoids outlier interference and the results have high reliability. The Mann–Kendall trend test defines the statistic S to quantify the expression of the trend, which for a given time series of data is calculated as follows [38,39]:

$$S = \sum_{i=1}^{n-1} \sum_{j=i+1}^n \text{sgn}(x_j - x_i), \quad (3)$$

where x_i and x_j denote values in periods i and j of the time-series data, respectively, and sgn takes the values:

$$\text{sgn}(x_j - x_i) = \begin{cases} 1 & (x_j - x_i > 0) \\ 0 & (x_j - x_i = 0) \\ -1 & (x_j - x_i < 0) \end{cases}. \quad (4)$$

When $n > 8$, the random sequence S approximately obeys the normal distribution, when $S > 0$, it indicates an upward trend, and when $S < 0$, it indicates a downward trend. The statistic value Z is then obtained by standardizing the sequence S to determine whether the upward or downward trend of the time-series data passes the significance level test, which is calculated by the following formula:

$$Z = \begin{cases} S - 1/\sqrt{\text{Var}(s)} & S > 0 \\ 0 & S = 0. \\ S + 1/\sqrt{\text{Var}(S)} & S < 0 \end{cases} \quad (5)$$

$\text{Var}(s)$ is calculated as:

$$\text{Var}(s) = \frac{n(n-1)(2n+5)}{18}. \quad (6)$$

Then, the M–K test is performed for the trend (confidence level is set at 95%), if $T - sen > 0$ and $p < 0.05$, it is significantly increased; if $T - sen > 0$ and $p > 0.05$, it is not significantly increased; if $T - sen < 0$ and $p < 0.05$, it is significantly decreased; if $T - sen < 0$ and $p > 0.05$, it is not significantly decreased.

2.5.3. Climate Sensitivity Analysis

To explore the relationship between TRW and EVI, we calculated Pearson correlations between TRW and EVI in six regions of the Qilian Mountains from 2000 to 2020. In the Qilian Mountains, drought has been an unfavorable factor for tree growth. In order to determine the main control factors affecting TRW and EVI, we calculated the Pearson correlation between TRW and each climatic factor from 1960 to 2020 and from 2000 to 2020, as well as the Pearson correlation between EVI and each climatic factor from 2000 to 2020. Finally, redundancy analysis (RDA) was performed for TRW, EVI and climate factors for the whole Qilian Mountains region. If the arrows of species and environmental factors are in the same direction, and the angle between the two arrows is acute, then there is a positive correlation between species and environmental factors; if they is in the opposite

direction and obtuse, then there is a negative correlation, while the larger the projection area in the direction of environmental factors, the stronger the correlation is.

3. Results

3.1. Comparison of Spatial and Temporal Patterns of Interannual Trends in Tree Radial Growth and EVI

During the 1960–1980 period, the trend in TRW showed an increasing trend in all study areas ($R^2 = 0.58–0.98$) (Figure 4). During the 1980–2000 period, the trend in TRW in the MH, WH, EL, ML, WL areas showed a decreasing trend ($R^2 = 0.88–0.97$), except for the EH area. During the 2000–2020 period, comparing the trends of TRW and EVI, we found that the TRW of the EH, MH, and WH areas showed an increasing trend at high elevation, especially the increase at WH, which was the most significant ($R^2 = 0.84–0.97$). In the same period, EVI also showed a trend consistent with TRW at high altitude where the rising trend of EVI in the WH area was also significant ($R^2 = 0.74–0.95$). At low elevation, we found that the changes in TRW and EVI were relatively stable in the EL and ML areas, but in the WL area, both TRW and EVI showed a significant increasing trend ($R^2 = 0.74–0.88$). The consistency of TRW and EVI trends at high and low elevation was stronger in the western region than in the eastern and middle regions. The trends of TRW and EVI changes gradually converged with an increase in regional aridity.

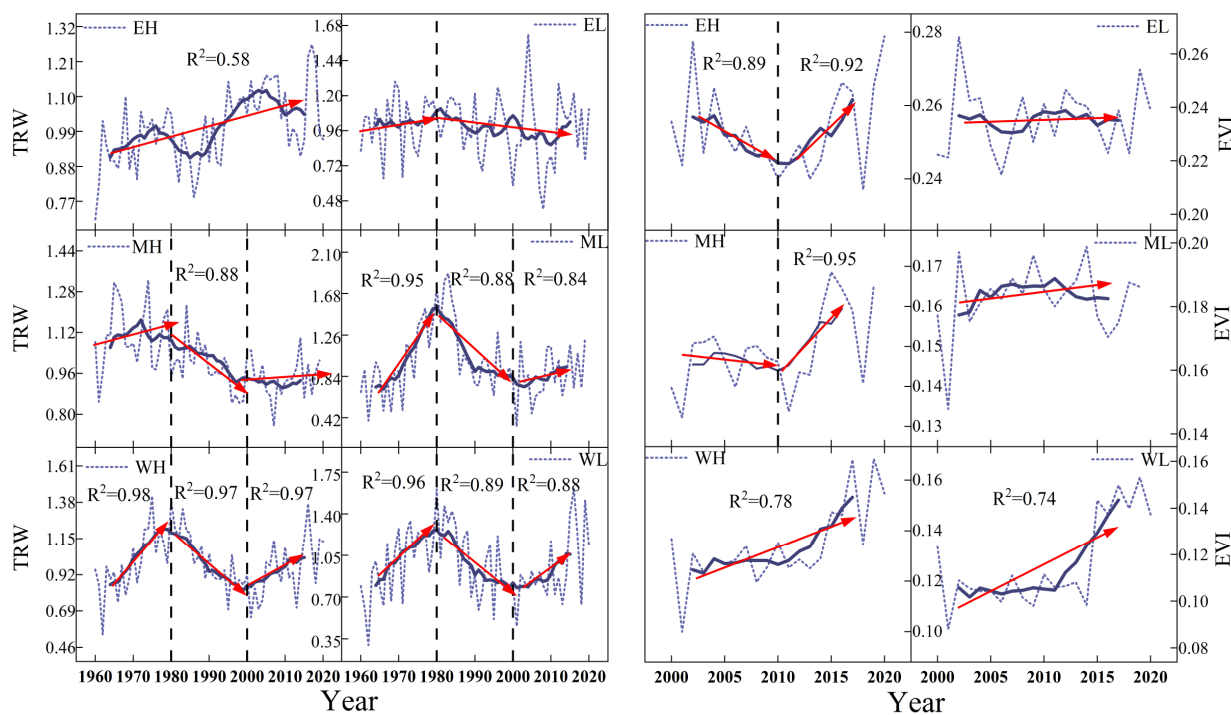


Figure 4. The trends of TRW from 1960 to 2020 and EVI from 2000 to 2020 (solid blue line—three-year sliding average, solid red line—linear regression).

During the past two decades, the spatial distribution of EVI trends in the study area indicate a general increase (Figure 5), which is consistent with the increase in tree growth recorded by tree rings. The EVI trend showed a growing trend, with 70.72% of the whole area showing a significant increase, and 29.27% showing a significant decrease.

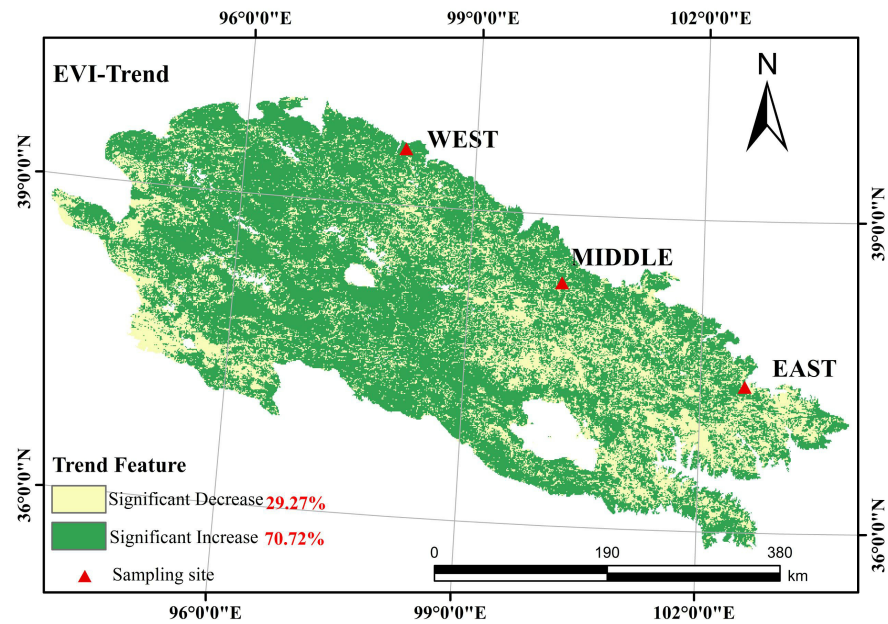


Figure 5. Spatial distribution of EVI trend in the Qilian Mountains from 2000 to 2020.

3.2. The Relationship between TRW and EVI

There was a positive correlation between TRW and EVI in the Qilian Mountains, and the relationship between TRW and EVI tended to be consistent with the increase in regional aridity (Figure 6). Specifically, in the eastern region, there was a lag effect between TRW and EVI at both high and low elevation. In the EH region, TRW and EVI showed a significant positive correlation at a three-year lag ($r = 0.47, p < 0.01$). In the EL region, there was a significant positive correlation between TRW and EVI at a two-year lag ($r = 0.50, p < 0.01$). In the middle region, there was a lag effect between TRW and EVI at high altitude, while TRW and EVI at low altitude showed a significant positive correlation in the current year. In the MH region, TRW and EVI presented a significant positive correlation at a two-year lag ($r = 0.67, p < 0.01$). Nevertheless, in the ML region, TRW in the current year was significantly positively correlated with EVI ($r = 0.45, p < 0.01$). In the western region, TRW and EVI at both high and low elevation were significantly and positively correlated in the current year ($r = 0.70\text{--}0.73, p < 0.01$).

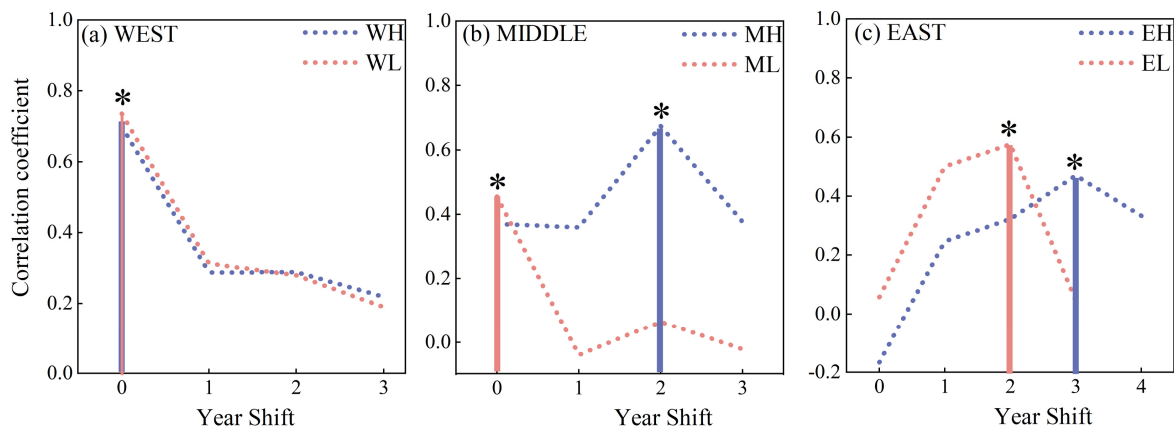


Figure 6. Correlations between TRW and EVI at two elevations of western (a), central (b) and eastern (c) regions of the Qilian Mountains from 2000 to 2020. * $p < 0.05$.

3.3. Response Analysis of TRW and EVI to Climate Factors

During the 2000–2020 period, the sensitivity of EVI to temperature factors decreased gradually with increasing regional drought, and the sensitivity to moisture factors increased gradually with increasing regional drought (Figure 7).

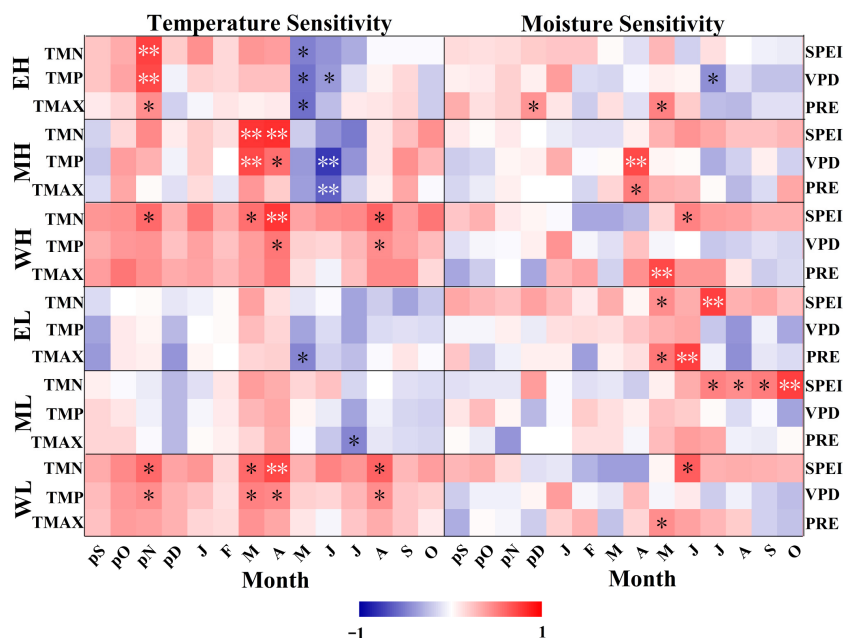


Figure 7. Correlations between EVI and climate factors from September of the previous year to October of the current year in the Qilian Mountain regions from 2000 to 2020 (P—previous year; TMN—mean minimum temperature; TMP—mean temperature; TMAX—mean maximum temperature; SPEI—standardized precipitation evapotranspiration index; VPD—vapor pressure deficit; PRE—precipitation). ** $p < 0.01$; * $p < 0.05$.

In the EH region, EVI was significantly and positively correlated with temperature in November of the previous year ($r = 0.582, p < 0.01$), there was a significant negative correlation with temperature in May ($r = -0.442, p < 0.05$), and there was a significant positive correlation with PRE from December of the previous year to May of the current year ($r = 0.489–0.515, p < 0.05$), but no significant correlation with SPEI. In the EL region, EVI was positively correlated with PRE from May to June of the current year ($r = 0.494–0.622, p < 0.05$) and it was also positively correlated with SPEI in May ($r = 0.455, p < 0.05$) and July of the current year ($r = 0.693, p < 0.01$). In the MH region, EVI was negatively correlated with temperature in June of the current year ($r = -0.605, p < 0.01$) and was correlated positively with PRE in April of current year ($r = 0.516, p < 0.05$). In the ML region EVI had a significantly negative correlation with temperature in July of the current year ($r = -0.477, p < 0.05$) and had a significantly positive correlation with SPEI from July to October of the current year ($r = 0.493–0.563, p < 0.05$). In the WH region, there was a significant positive correlation between EVI and temperature in April of the current year ($r = 0.613, p < 0.01$) and EVI was positively correlated with PRE in May of the current year ($r = 0.601, p < 0.01$) and was positively correlated with SPEI in June of the current year ($r = 0.446, p < 0.05$). In the WL region, EVI had a significant positive correlation with PRE in May of the current year ($r = 0.463, p < 0.05$) and there was also a significant positive correlation between EVI and SPEI in June of the current year ($r = 0.457, p < 0.05$).

Compared with the correlations between EVI and climate factors, we found that TRW are less sensitive to climate than EVI (Figure 8). There was no significant correlation between TRW and temperature in the EL, MH, and ML regions. In the EH region, TRW had a significant negative correlation with TMN in April of the current year ($r = 0.413, p < 0.05$). During the growing season, there was no significant correlation between TRW and PRE in

the EH region, while in the EL region, TRW was positively correlated with PRE in July of the current year ($r = 0.514, p < 0.05$). In the ML region, TRW was correlated positively with PRE in May of current year ($r = 0.602, p < 0.01$) as well as with SPEI in June to October of current year ($r = 0.502\text{--}0.626, p < 0.05$). In the WH region, TRW had a significant positive correlation with PRE in May of the current year ($r = 0.444, p < 0.05$). In the WL region, TRW was correlated positively with PRE in May of the current year ($r = 0.639, p < 0.01$) and with SPEI from May to June of the current year ($r = 0.461\text{--}0.482, p < 0.05$).

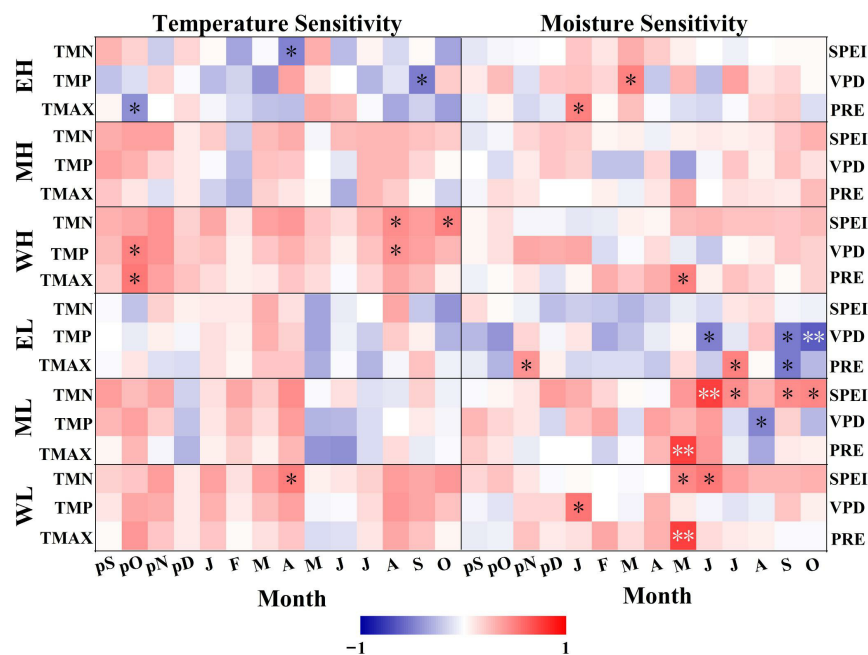


Figure 8. Correlations between TRW and climate factors from September of the previous year to October of the current year in the Qilian Mountain regions from 2000 to 2020. ** $p < 0.01$; * $p < 0.05$.

The sensitivity of TRW to climate was weaker for short time series; in order to find the main control factors affecting TRW, we further analyzed the sensitivity of TRW to climate for a long time series from 1960 to 2020 (Figure 9).

The sensitivity of TRW to moisture factors gradually increased with the increase in regional drought from 1960 to 2020. In the EH region, TRW was negatively correlated with temperature in June of the current year ($r = -0.352, p < 0.01$) but positively correlated with SPEI in May of the current year ($r = 0.276, p < 0.05$). In the EL region, TRW was negatively correlated with temperature from June to July of the current year ($r = -0.362\text{--}0.274, p < 0.05$), while it was positively correlated with SPEI from May to August of the current year ($r = 0.263\text{--}0.304, p < 0.05$). In the MH region, TRW had a significant negative correlation with temperature in June of the current year ($r = -0.241, p < 0.01$). In the ML region, there was a significant negative correlation between TRW and temperature from June to July of the current year ($r = -0.374\text{--}0.237, p < 0.05$), while TRW was positively correlated with PRE in June of the current year ($r = 0.342, p < 0.01$) and with SPEI from June to September of the current year ($r = 0.267\text{--}0.387, p < 0.05$). In the WH region, TRW was positively correlated with PRE in June of the current year ($r = 0.243, p < 0.05$), and it also positively correlated with SPEI from September to November of the previous year as well as from June to October of the current year ($r = 0.262\text{--}0.386, p < 0.01$). In the WL region, TRW was negatively correlated with temperature in June of the current year ($r = -0.408, p < 0.05$), while it was positively correlated with PRE from May to June of the current year ($r = 0.302\text{--}0.404, p < 0.01$), with SPEI from September to November of the previous year as well as from May to October of the current year ($r = 0.332\text{--}0.605, p < 0.01$).

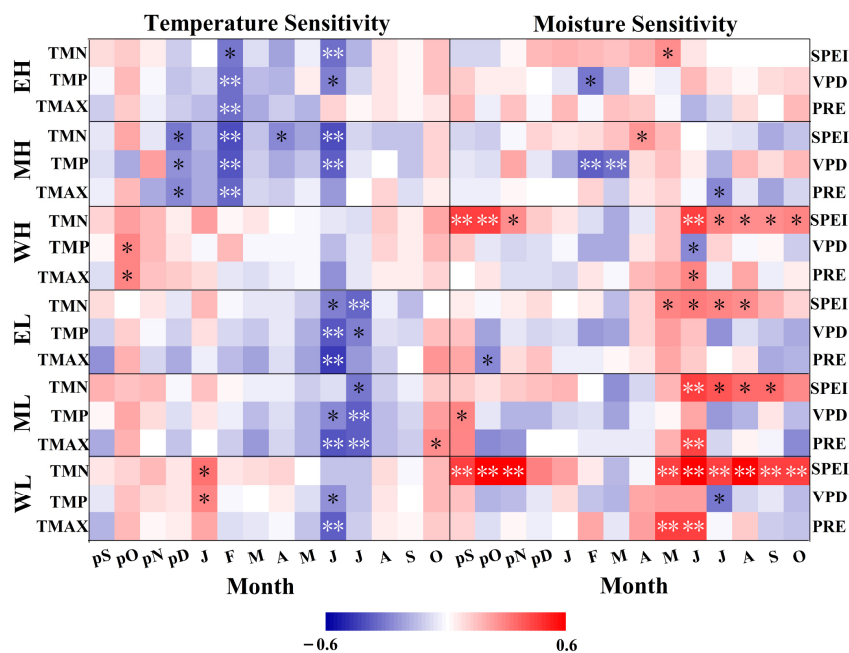


Figure 9. Correlations between TRW and climate factors from September of the previous year to October of the current year in the Qilian Mountain regions from 1960 to 2020. ** $p < 0.01$; * $p < 0.05$.

Finally, we investigated the relationship between TRW, EVI and climate factors in the whole Qilian Mountain region by redundancy analysis (RDA) (Figure 10). SPEI was the driving factor affecting both TRW and EVI in the low elevation regions. The contribution of SPEI to TRW at low elevation was 10.9%, the contribution of TMAX to TRW at high elevation was 73.2%, the contribution of SPEI to EVI at low elevation was 74.2% and the contribution of VPD to EVI was 11.7%. Therefore, we assumed that the greater the drought intensity, the more consistent the driving factors affecting TRW and EVI were. Compared to low elevation, tree growth at high elevation in the Qilian Mountains is influenced by many factors; temperature is one of the factors affecting tree growth at high elevation in the Qilian Mountains.

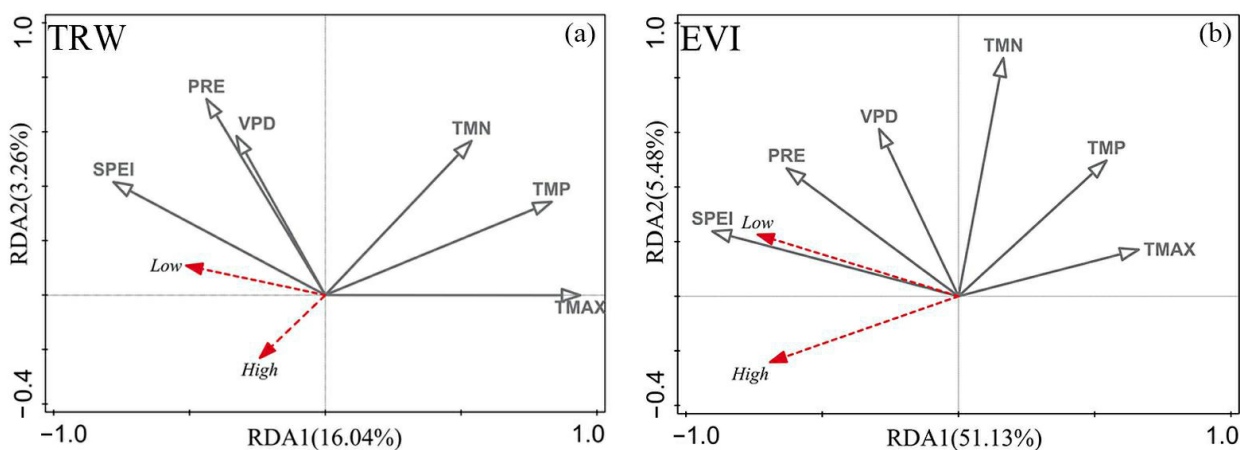


Figure 10. (a) Redundancy analysis of TRW and each climate factor in the Qilian Mountains region from 1960 to 2020 and (b) redundancy analysis of EVI and each climate factor in the Qilian Mountains region from 2000 to 2020 (High—high elevation; Low—low elevation; TMN—mean minimum temperature; TMP—mean temperature; TMAX—mean maximum temperature; SPEI—standardized precipitation evapotranspiration index; VPD—vapor pressure deficit; PRE—precipitation).

4. Discussion

4.1. Spatial and Temporal Patterns of Interannual Variation of TRW and EVI

Our study found an overall increasing trend in TRW in the Qilian Mountains over the past 60 years. However, there was a decreasing trend in TRW from 1980 to 2000 (Figure 4). This is consistent with previous studies in the Qilian Mountains [29]. Both EVI and TRW showed an overall increasing trend in the last 20 years, and the trends in TRW and EVI gradually coincided with the increase in regional drought degree; significant global warming has occurred since the 1990s, and this warming trend is still increasing and forecast to be further enhanced in the coming decades [40]. From 1960 to 1980, the climate in the Qilian Mountains warmed slowly and the increase in precipitation led to a wet trend during this period, thus promoting tree growth throughout the region. During the period 1980–2000, temperature increased throughout the Qilian Mountains, precipitation increased steadily in the east, and decreased in the middle and western areas. At high elevations in the Qilian Mountains where low temperatures limit tree growth, warming will promote photosynthesis and carbon accumulation, which will have a positive effect on tree growth if the tree habitat is moist enough [41]. Therefore, in the more humid regions of the Qilian Mountains, raised temperatures instead promoted tree growth. While a tree habitat is under water stress, an increase in temperature aggravates drought stress, causing evaporation of soil water, root water shortage, and excessive water loss in trees leading to closed or partially closed stomata, which also reduces the photosynthetic efficiency of trees. At the same time, the leaf and root respiratory intensity will consume more and more limited organic compounds accumulated during photosynthesis [42,43]. These all can affect the physiological activity of the tree. In the Qilian Mountains, where water stress is more severe, elevated temperatures and reduced precipitation have aggravated drought stress in these regions [44], so that they have limited the growth of trees. The decreasing trend of TRW gradually worsened as the regional drought intensity increased.

The IPCC report [1] has shown that there has been a global warming hiatus since 2000. In the study of radial growth change in trees, it showed that warming halted and a relative wetting trend may have had a significant impact on tree and forest growth in the Northern Hemisphere [28]. Our results found that the alleviation of drought stress greatly promoted the growth of western Qinghai spruce from 2000 to the present. The TRW and EVI both showed increasing trends in the Qilian Mountains. There are two reasons for the increase in EVI and TRW in the Qilian Mountains region from 2000 to 2020: (i) the decrease in warming and the trend in EVI from 2000 to the present confirmed the wet conditions reflected by the increase in precipitation. This has alleviated drought stress to some extent, and has promoted tree growth as well as an increased the greening trend; (ii) the extension of the growing season. An extended growing season will accelerate tree growth, especially for forests at high elevation and high latitude [12,45]. A study in the Qilian Mountains [46], which applied the Vaganov–Shashkin (VS)-oscilloscope model to analyze tree phenology of Qinghai spruce from 1960 to 2016, found that radial growth of Qinghai spruce showed a trend of an earlier start of the growing season and later end of growing season. With the elevated temperature and increased precipitation, tree growth time increased, which led to an increase in radial growth and EVI. By comparing the trends of TRW and EVI, the tendency of EVI to rise is stronger than that of TRW, and we predict that if global temperature continues to rise and wetness decreases, the growth of Qilian Mountain Qinghai spruce trees and forest canopy will show a decreasing trend in the future, and the EVI will decrease to a greater degree, with both of them being exposed to an increased degree of drought stress. Consequently, there is a great need to continue to monitor the dynamics of forests, especially in areas that are more severely affected by drought stress; these efforts should be strengthened to monitor EVI. In order to better protect and manage forests, the focus should be on changes in regional climate and tree phenology and utilizing tree physiological models to study the response relationships between regional climate changes and trees and forests.

4.2. Spatial and Temporal Patterns of TRW and EVI Relationships

There is a close relationship between net primary production and forest growth [47–49]; it has also been shown that satellite vegetation indices can be used as proxies for forest health and biomass [50] and there is a high correlation between normalized difference vegetation (NDVI) and EVI. Our study found a significant positive correlation between TRW and EVI ($p < 0.05$), and the consistency and synchrony of the positive correlation gradually increased with increasing drought stress, but the positive correlation had a lag effect. This is consistent with previous studies that explored the correlation between TRW and vegetation indices [16,21,51–53]. In Spain, a recent study on the relationship between TRW and NDVI suggested a general positive correlation between interannual variation in NDVI and TRW, with the relationship varying greatly between forest types and environmental conditions, and the drier the region, the stronger the relationship between vegetation index and TRW [54]. In Cyprus, a study showed elevational differences in the relationship between TRW and NDVI, and that tree rings and vegetation index may not be as strongly linked at higher elevations. However, TRW in low elevation arid regions is closely related to NDVI [55]. All these studies have shown that TRW is poorly correlated with vegetation index in wet areas, while drought stress strengthens the consistency of the TRW and vegetation index relationships in moisture-limited areas.

It has been suggested that increases in biomass and long-term stored carbon do not depend on the photosynthetic rate, but on how the trunk and branches, as well as the below-ground components grow and form wood. This makes the storage of long-lived biomass in the woody fraction of trees physically and temporally separate from the leaf-carbon gain quantified by satellite vegetation indices [56]. Meantime carbon will be used first for primary growth in order to form new shoots, buds, leaves and roots [57] at the same time as xylogenesis from the expansion to the lignification of wood cells, where there is a time lag in the wood formation process [58]. This suggests that there is a correlation between TRW and EVI, and there is a lag in the correlation between both. The reasons for the differences in spatial and temporal patterns of the positive correlation between TRW and EVI include two aspects. In terms of climate change analysis, there was a study showing that different forest types, regional climatic and environmental conditions produce different patterns in the relationship between TRW and vegetation index [16]. This suggests that differences in regional climatic and environmental conditions can lead to significant differences in the relationship between TRW and EVI. In eastern and high elevation areas where there could be more water from rain and snow melt, the water limitation would be less than that in low elevation areas, so the correlation between TRW and vegetation index would not be as strong as in eastern and high elevation areas. However, both vegetation index and TRW were limited by drought in arid and low elevation areas, and drought stress enhanced the synchronization of TRW with vegetation index [59]. Analyzing from a tree physiology perspective, it has been suggested that tree activity will affect TRW in the following growing season in low moisture-limited areas [60]. The lag effect from the previous year may affect tree growth in the following years [61,62]. In addition, trees synthesize and store excess carbohydrates, and trees use the stored carbon primarily for cell-wall thickening processes or in non-structural carbohydrate reserves above and below ground as a support for the next year's tree growth [63]. The significant positive correlation between TRW and EVI at a lag of 2–3 years in the humid Qilian Mountains also validates the expectation of a study that carbon stocks which formed several years ago may have an impact on tree growth [64]. In the driest regions, xylem production is limited to one season [65] and its production will be limited by soil-water availability and photoperiod. These characteristics will probably limit the linkage between tree growth and photosynthesis more during the short-term period when water is available [16]; this explains why there was a significant positive correlation between EVI and TRW in the current year in the Qilian Mountains, which are severely stressed by drought.

4.3. Spatial and Temporal Differences in the Sensitivity of TRW and EVI to Climate Change

In our study, by comparing the sensitivity of EVI and TRW to climate factors from 2000 to 2020, we found that the sensitivity of EVI to climate factors was stronger than that of TRW, and the growth trend of EVI in the Qilian Mountains was more variable than that of TRW; in addition, the correlation between EVI and climate factors from 2000 to 2020 was significantly stronger than that for TRW. One reason is that remote sensing can directly reflect plant-growth information, while TRW is a reflection of vegetation-growth conditions and their environmental change processes over longer time scales [66]. Another reason is that in arid regions, leaf stomatal regulation is the first line to defend plants against water stress [67]. The Qilian Mountains are located in the northwestern arid zone, and when water stress intensifies with increasing temperature, plants close leaf stomata through feedback regulation, reducing transpiration rates, which is a drought avoidance mechanism for plants.

The sensitivity of EVI and TRW to climate gradually strengthened with the increase in regional aridity. A study in semi-arid forests of inner Asia has shown that trees in dry regions are more sensitive to climate than those in wet regions [68]. Our study found that the magnitude of the trend variation of TRW and EVI was enhanced with the increase in regional aridity, while the correlation between EVI, TRW and climate factors reached a significant number gradually increasing with the increase in regional aridity. This all represents a greater sensitivity to climate for trees in dry areas of the Midwest and lower elevations than for trees in eastern regions and higher elevations, which is consistent with previous findings [68,69]. This is because organisms have different mechanisms and strategies for adapting to environmental changes in different environments. In regions with severe drought stress, hydraulic failure and reduction in carbon acquisition, thus reducing tree resistance, leads to increased susceptibility to drought in the Midwest, so that the decline in tree growth trends is greater and climate factors are more limiting at lower elevation in the Midwest than in the East. Trees from arid areas are less resistant, but recover faster than trees from wet areas [70], and are more sensitive to water availability than trees from wet areas; thus, as drought stress in the Qilian Mountains diminished over the last two decades, the greatest increase in tree growth trends occurred at lower elevation in the western region.

Droughts caused by global warming over the past two decades have led to the decline and death of trees in areas such as inland Asia and western Canada [68,71–74]. Studies in areas such as high elevations of western North America and central Europe have shown that warming extends the growing season, accelerates tree growth and increases forest biomass in these areas [11–13,75,76]. Meanwhile, research has shown that global warming increases vegetation greenness and Arctic biomes in the boreal region while decreasing vegetation greenness in the tropics [77]. In the Qilian Mountains region, research has shown a significant increase in vegetation index in most of the study area since the 2010s [29]. According to our study, we concluded that the coupling relationship between EVI and TRW and the response to climate change tended to be consistent in dry areas, with both TRW and EVI serving as good proxies for the response of forests to climate change. However, in wetter areas, EVI is more sensitive to climate change. Therefore, in future forest management and protection efforts, the dynamics of TRW and EVI should be monitored simultaneously for dry areas, while the dynamics of EVI should be the focus of monitoring for wetter areas. In parallel, for sudden droughts and natural disasters, we should give priority to monitoring changes in EVI. Moreover, for studying the response of tree growth to climate change at long time scales, we should strengthen monitoring of the dynamics of TRW.

5. Conclusions

In this study, we combined tree-ring data with remote sensing data to compare the interannual trends of TRW and EVI, and analyzed the characteristics of the relationship between TRW and EVI from 2000 to 2020, as well as the spatial and temporal differences in their responses to climate factors. The spatial and temporal patterns of interannual

variation of TRW and EVI over the last two decades indicate that the current climate change is favorable for growth of vegetation in the Qilian Mountains, and the interannual variation of TRW and EVI tends to be consistent with the increase in regional aridity. Enhanced monitoring of tree growth and greening trends will facilitate more accurate predictions of future climate change in forest process-based climate models. The spatial and temporal patterns of TRW and EVI relationships indicate that the positive correlation between TRW and EVI is geographically patterned, and their coupling becomes stronger as regional aridity increases. In future forest management and conservation, both TRW and EVI should be monitored with emphasis on areas where drought stress is severe, while in areas where environmental conditions are suitable for forest growth, TRW and EVI should be monitored differently. The spatial and temporal differences in the sensitivity of TRW and EVI to climate change indicate that the correlation between TRW and temperature and humidity factors decreased from 2000 to the present, and drought stress in the Qilian Mountains has been alleviated. The main controlling climate factors which influence TRW and EVI changes from east to west and from high to low elevation gradually converge. In the future, forest management, such as management of tree water use and anthropogenic intervention, should be strengthened in western and low elevation areas. Meanwhile, in future research on forest management and conservation, the focus should be on formative layer phenology and wood formation at finer time scales, combining them with remote sensing data, as well as incorporating models which can predict climate change and models based on tree physiology; this would be helpful in formulating timely and effective forest management policies and predicting how forests will respond to future climate change.

Author Contributions: Conceptualization, M.W. and L.J.; methodology, M.W.; software, M.W.; validation, M.W. and L.J.; formal analysis, M.W.; investigation, M.W., L.J., X.W., P.Z., D.D. and R.X.; resources, M.W. and L.J.; data curation, M.W. and L.J.; writing—original draft preparation, M.W. and L.J.; writing—review and editing, M.W. and L.J.; visualization, X.W., P.Z., D.D. and R.X.; supervision, L.J., X.W., P.Z., D.D. and R.X.; project administration, M.W. and L.J.; funding acquisition, L.J. All authors have read and agreed to the published version of the manuscript.

Funding: This research was supported by the CAS “Light of West China” Program (Funder: Liang Jiao; 2020XBZG-XBQNXZ-A), the National Natural Science Foundation of China (Funder: Liang Jiao; Grant No. 41861006), and the Research Ability Promotion Program for Young Teachers of Northwest Normal University (Funder: Liang Jiao; NWNNU-LKQN2019-4).

Data Availability Statement: All data files are available from the Open Science Framework (OSF): DOI 10.17605/OSF.IO/TM5HC.

Conflicts of Interest: The authors declare no conflict of interest.

References

1. Masson-Delmotte, V.; Zhai, P.; Pirani, A.; Connors, S.L.; Péan, C.; Berger, S.; Caud, N.; Chen, Y.; Goldfarb, L.; Gomis, M.; et al. *Climate Change 2021: The Physical Science Basis*; Cambridge University Press: Cambridge, UK, 2021. [[CrossRef](#)]
2. Allen, M.; Antwi-Agyei, P.; Aragon-Durand, F. *Technical Summary: Global Warming of 1.5 C. An IPCC Special Report on the Impacts of Global Warming of 1.5 C above Pre-Industrial Levels and Related Global Greenhouse Gas Emission Pathways, in the Context of Strengthening the Global Response to the Threat of Climate Change, Sustainable Development, and Efforts to Eradicate Poverty*; Intergovernmental Panel on Climate Change: Geneva, Switzerland, 2019.
3. Bonan, G.B. Forests and climate change: Forcings, feedbacks, and the climate benefits of forests. *Science* **2008**, *320*, 1444–1449. [[CrossRef](#)]
4. Seidl, R.; Thom, D.; Kautz, M.; Martin-Benito, D.; Peltoniemi, M.; Vacchiano, G.; Wild, J.; Ascoli, D.; Petr, M.; Honkaniemi, J.; et al. Forest disturbances under climate change. *Nat. Clim. Chang.* **2017**, *7*, 395–402. [[CrossRef](#)]
5. Camarero, J.J.; Gazol, A.; Sangüesa-Barreda, G.; Oliva, J.; Vicente-Serrano, S.M.; Gibson, D. To die or not to die: Early warnings of tree dieback in response to a severe drought. *J. Ecol.* **2015**, *103*, 44–57. [[CrossRef](#)]
6. Gazol, A.; Camarero, J.J.; Anderegg, W.R.L.; Vicente-Serrano, S.M. Impacts of droughts on the growth resilience of Northern Hemisphere forests. *Glob. Ecol. Biogeogr.* **2017**, *26*, 166–176. [[CrossRef](#)]
7. Gea-Izquierdo, G.; Nicault, A.; Battipaglia, G.; Dorado-Linan, I.; Gutierrez, E.; Ribas, M.; Guiot, J. Risky future for Mediterranean forests unless they undergo extreme carbon fertilization. *Glob. Chang. Biol.* **2017**, *23*, 2915–2927. [[CrossRef](#)]

8. Hudson, J.M.; Henry, G.H. Increased plant biomass in a High Arctic heath community from 1981 to 2008. *Ecology* **2009**, *90*, 2657–2663. [[CrossRef](#)]
9. Sánchez-Salguero, R.; Navarro-Cerrillo, R.M.; Camarero, J.J.; Fernández-Cancio, Á. Selective drought-induced decline of pine species in southeastern Spain. *Clim. Chang.* **2012**, *113*, 767–785. [[CrossRef](#)]
10. Sarris, D.; Christodoulakis, D.; KÖRner, C. Recent decline in precipitation and tree growth in the eastern Mediterranean. *Glob. Chang. Biol.* **2007**, *13*, 1187–1200. [[CrossRef](#)]
11. McMahon, S.M.; Parker, G.G.; Miller, D.R. Evidence for a recent increase in forest growth. *Proc. Natl. Acad. Sci. USA* **2010**, *107*, 3611–3615. [[CrossRef](#)]
12. Pretzsch, H.; Biber, P.; Schütze, G.; Uhl, E.; Rotzer, T. Forest stand growth dynamics in Central Europe have accelerated since 1870. *Nat. Commun.* **2014**, *5*, 4967. [[CrossRef](#)]
13. Salzer, M.W.; Hughes, M.K.; Bunn, A.G.; Kipfmüller, K.F. Recent unprecedented tree-ring growth in bristlecone pine at the highest elevations and possible causes. *Proc. Natl. Acad. Sci. USA* **2009**, *106*, 20348–20353. [[CrossRef](#)]
14. Babst, F.; Bouriaud, O.; Alexander, R.; Trouet, V.; Frank, D. Toward consistent measurements of carbon accumulation: A multi-site assessment of biomass and basal area increment across Europe. *Dendrochronologia* **2014**, *32*, 153–161. [[CrossRef](#)]
15. Babst, F.; Bouriaud, O.; Papale, D.; Gielen, B.; Janssens, I.A.; Nikinmaa, E.; Ibrom, A.; Wu, J.; Bernhofer, C.; Kostner, B.; et al. Above-ground woody carbon sequestration measured from tree rings is coherent with net ecosystem productivity at five eddy-covariance sites. *New Phytol.* **2014**, *201*, 1289–1303. [[CrossRef](#)]
16. Vicente-Serrano, S.M.; Camarero, J.J.; Olano, J.M.; Martín-Hernández, N.; Peña-Gallardo, M.; Tomás-Burguera, M.; Gazol, A.; Azorin-Molina, C.; Bhuyan, U.; El Kenawy, A. Diverse relationships between forest growth and the Normalized Difference Vegetation Index at a global scale. *Remote Sens. Environ.* **2016**, *187*, 14–29. [[CrossRef](#)]
17. Wong, C.Y.S.; Young, D.J.N.; Latimer, A.M.; Buckley, T.N.; Magney, T.S. Importance of the legacy effect for assessing spatiotemporal correspondence between interannual tree-ring width and remote sensing products in the Sierra Nevada. *Remote Sens. Environ.* **2021**, *265*, 112635. [[CrossRef](#)]
18. Andreu-Hayles, L.; D'Arrigo, R.; Anchukaitis, K.J.; Beck, P.S.A.; Frank, D.; Goetz, S. Varying boreal forest response to Arctic environmental change at the Firth River, Alaska. *Environ. Res. Lett.* **2011**, *6*, 045503. [[CrossRef](#)]
19. Bunn, A.G.; Hughes, M.K.; Kirilyanov, A.V.; Losleben, M.; Shishov, V.V.; Berner, L.T.; Oltchev, A.; Vaganov, E.A. Comparing forest measurements from tree rings and a space-based index of vegetation activity in Siberia. *Environ. Res. Lett.* **2013**, *8*, 035034. [[CrossRef](#)]
20. Kaufmann, R.K.; D'Arrigo, R.D.; Paletta, L.F.; Tian, H.Q.; Jolly, W.M.; Myneni, R.B. Identifying Climatic Controls on Ring Width: The Timing of Correlations between Tree Rings and NDVI. *Earth Interact.* **2008**, *12*, 1–14. [[CrossRef](#)]
21. Lopatin, E.; Kolstrom, T.; Spiecker, H. Determination of forest growth trends in Komi Republic (northwestern Russia): Combination of tree-ring analysis and remote sensing data. *Boreal Environ. Res.* **2006**, *11*, 341–353.
22. Beck, P.S.A.; Andreu-Hayles, L.; D'Arrigo, R.; Anchukaitis, K.J.; Tucker, C.J.; Pinzón, J.E.; Goetz, S.J. A large-scale coherent signal of canopy status in maximum latewood density of tree rings at arctic treeline in North America. *Glob. Planet. Chang.* **2013**, *100*, 109–118. [[CrossRef](#)]
23. Berner, L.T.; Beck, P.S.A.; Bunn, A.G.; Lloyd, A.H.; Goetz, S.J. High-latitude tree growth and satellite vegetation indices: Correlations and trends in Russia and Canada (1982–2008). *J. Geophys. Res.* **2011**, *116*, G01015. [[CrossRef](#)]
24. Brehaut, L.; Danby, R.K. Inconsistent relationships between annual tree ring-widths and satellite-measured NDVI in a mountainous subarctic environment. *Ecol. Indic.* **2018**, *91*, 698–711. [[CrossRef](#)]
25. Correa-Diaz, A.; Silva LC, R.; Horwath, W.R.; Gómez-Guerrero, A.; Vargas-Hernández, J.; Villanueva-Díaz, J.; Suárez-Espinoza, J. Linking Remote Sensing and Dendrochronology to Quantify Climate-Induced Shifts in High-Elevation Forests Over Space and Time. *J. Geophys. Res. Biogeosci.* **2019**, *124*, 166–183. [[CrossRef](#)]
26. Zhou, Y.; Yi, Y.; Jia, W.; Cai, Y.; Yang, W.; Li, Z. Applying dendrochronology and remote sensing to explore climate-drive in montane forests over space and time. *Quat. Sci. Rev.* **2020**, *237*, 106292. [[CrossRef](#)]
27. Seftigen, K.; Frank, D.C.; Björklund, J.; Babst, F.; Poulter, B. The climatic drivers of normalized difference vegetation index and tree-ring-based estimates of forest productivity are spatially coherent but temporally decoupled in Northern Hemispheric forests. *Glob. Ecol. Biogeogr.* **2018**, *27*, 1352–1365. [[CrossRef](#)]
28. Gao, L.; Gou, X.; Deng, Y.; Yang, M.; Zhao, Z.; Cao, Z. Dendroclimatic Response of *Picea crassifolia* along an Altitudinal Gradient in the Eastern Qilian Mountains, Northwest China. *Arct. Antarct. Alp. Res.* **2018**, *45*, 491–499. [[CrossRef](#)]
29. Gao, L.; Gou, X.; Deng, Y.; Wang, Z.; Gu, F.; Wang, F. Increased growth of Qinghai spruce in northwestern China during the recent warming hiatus. *Agric. For. Meteorol.* **2018**, *260–261*, 9–16. [[CrossRef](#)]
30. Zhao, C.; Chen, L.; Ma, F.; Yao, B.; Liu, J. Altitudinal differences in the leaf fitness of juvenile and mature alpine spruce trees (*Picea crassifolia*). *Tree Physiol.* **2008**, *28*, 133–141. [[CrossRef](#)]
31. Yang, M.H.; Melvin, T.M.; Zhao, Y.; Briffa, K.R. Climate Control on Tree Growth at the Upper and Lower Treelines: A Case Study in the Qilian Mountains, Tibetan Plateau. *PLoS ONE* **2013**, *8*, e69065. [[CrossRef](#)]
32. Zhang, J.; Gou, X.; Zhang, Y.; Lu, M.; Xu, X.; Zhang, F.; Liu, W.; Gao, L. Forward modeling analyses of Qilian Juniper (*Sabina przewalskii*) growth in response to climate factors in different regions of the Qilian Mountains, northwestern China. *Trees* **2016**, *30*, 175–188. [[CrossRef](#)]
33. Holmes, R.L. Computer-Assisted Quality Control in Tree-Ring Dating and Measurement. *Tree-Ring Bull.* **1983**, *43*, 51–67.

34. Cook, E.R.; Esper, J.; D'Arrigo, R.D. Extra-tropical Northern Hemisphere land temperature variability over the past 1000 years. *Quat. Sci. Rev.* **2004**, *23*, 2063–2074. [[CrossRef](#)]
35. Schweingruber, F.H. *Tree Rings: Basics and Applications of Dendrochronology*; Kluwer Academic Publishers: Norwell, MA, USA, 1988.
36. Thiel, H. A rank-invariant method of linear and polynomial regression analysis. *Indag. Math.* **1950**, *12*, 173.
37. Sen, P.K. Estimates of the Regression Coefficient Based on Kendall's Tau. *J. Am. Stat. Assoc.* **1968**, *63*, 1379–1389. [[CrossRef](#)]
38. Kendall, M.G. Rank Correlation Methods. *Br. J. Psychol.* **1990**, *25*, 86–91. [[CrossRef](#)]
39. Mann, H.B. Nonparametric tests against trend. *Econometrica* **1945**, *13*, 245–259. [[CrossRef](#)]
40. Huang, J.P.; Yu, H.P.; Guan, X.D.; Wang, G.Y.; Guo, R.X. Accelerated dryland expansion under climate change. *Nat. Clim. Chang.* **2016**, *6*, 166–171. [[CrossRef](#)]
41. Dusenge, M.E.; Duarte, A.G.; Way, D.A. Plant carbon metabolism and climate change: Elevated CO₂ and temperature impacts on photosynthesis, photorespiration and respiration. *New Phytol.* **2019**, *221*, 32–49. [[CrossRef](#)]
42. Rodríguez-Calcerrada, J.; Shahin, O.; Del Carmen Del Rey, M.A.; Rambal, S. Opposite changes in leaf dark respiration and soluble sugars with drought in two Mediterranean oaks. *Funct. Plant Biol.* **2011**, *38*, 1004–1015. [[CrossRef](#)]
43. Wehr, R.; Munger, J.W.; McManus, J.B.; Nelson, D.D.; Zahniser, M.S.; Davidson, E.A.; Wofsy, S.C.; Saleska, S.R. Seasonality of temperate forest photosynthesis and daytime respiration. *Nature* **2016**, *534*, 680–683. [[CrossRef](#)]
44. Jiao, L.; Jiang, Y.; Wang, M.; Zhang, W.; Zhang, Y. Age-Effect Radial Growth Responses of *Picea schrenkiana* to Climate Change in the Eastern Tianshan Mountains, Northwest China. *Forests* **2017**, *8*, 294. [[CrossRef](#)]
45. Chmielewski, F.-M.; Rötzer, T. Response of tree phenology to climate change across Europe. *Agric. For. Meteorol.* **2001**, *108*, 101–112. [[CrossRef](#)]
46. Xue, R.; Jiao, L.; Qi, C.; Chen, K.; Liu, X.; Du, D.; Wu, X. Growth and response patterns of *Picea crassifolia* and *Pinus tabuliformis* to climate factors in the Qilian Mountains, northwest China. *Dendrochronologia* **2022**, *71*, 125905. [[CrossRef](#)]
47. Babst, F.; Poulter, B.; Trouet, V.; Tan, K.; Neuwirth, B.; Wilson, R.; Carrer, M.; Grabner, M.; Tegel, W.; Levanic, T.; et al. Site- and species-specific responses of forest growth to climate across the European continent. *Glob. Ecol. Biogeogr.* **2013**, *22*, 706–717. [[CrossRef](#)]
48. Poulter, B.; Pederson, N.; Liu, H.; Zhu, Z.; D'Arrigo, R.; Ciais, P.; Davi, N.; Frank, D.; Leland, C.; Myneni, R.; et al. Recent trends in Inner Asian forest dynamics to temperature and precipitation indicate high sensitivity to climate change. *Agric. For. Meteorol.* **2013**, *178–179*, 31–45. [[CrossRef](#)]
49. Vicente-Serrano, S.M.; Camarero, J.J.; Zabalza, J.; Sangüesa-Barreda, G.; López-Moreno, J.I.; Tague, C.L. Evapotranspiration deficit controls net primary production and growth of silver fir: Implications for Circum-Mediterranean forests under forecasted warmer and drier conditions. *Agric. For. Meteorol.* **2015**, *206*, 45–54. [[CrossRef](#)]
50. Decuyper, M.; Chávez, R.O.; Čufar, K.; Estay, S.A.; Clevers, J.G.P.W.; Prislán, P.; Gričar, J.; Črepinšek, Z.; Merela, M.; de Luis, M.; et al. Spatio-temporal assessment of beech growth in relation to climate extremes in Slovenia—An integrated approach using remote sensing and tree-ring data. *Agric. For. Meteorol.* **2020**, *287*, 107925. [[CrossRef](#)]
51. Berner, L.T.; Beck, P.S.A.; Bunn, A.G.; Goetz, S.J. Plant response to climate change along the forest-tundra ecotone in northeastern Siberia. *Glob. Chang. Biol.* **2013**, *19*, 3449–3462. [[CrossRef](#)]
52. Leavitt, S.W.; Chase, T.N.; Rajagopalan, B.; Lee, E.; Lawrence, P.J. Southwestern U.S. tree-ring carbon isotope indices as a possible proxy for reconstruction of greenness of vegetation. *Geophys. Res. Lett.* **2008**, *35*, L12704. [[CrossRef](#)]
53. Lloyd, A.H.; Bunn, A.G.; Berner, L. A latitudinal gradient in tree growth response to climate warming in the Siberian taiga. *Glob. Chang. Biol.* **2011**, *17*, 1935–1945. [[CrossRef](#)]
54. Vicente-Serrano, S.M.; Martín-Hernández, N.; Camarero, J.J.; Gazol, A.; Sánchez-Salguero, R.; Peña-Gallardo, M.; El Kenawy, A.; Domínguez-Castro, F.; Tomas-Burguera, M.; Gutiérrez, E.; et al. Linking tree-ring growth and satellite-derived gross primary growth in multiple forest biomes. Temporal-scale matters. *Ecol. Indic.* **2020**, *108*, 105753. [[CrossRef](#)]
55. Coulthard, B.L.; Touchan, R.; Anchukaitis, K.J.; Meko, D.M.; Sivrikaya, F. Tree growth and vegetation activity at the ecosystem-scale in the eastern Mediterranean. *Environ. Res. Lett.* **2017**, *12*, 084008. [[CrossRef](#)]
56. Huston, M.A.; Wolverton, S. The global distribution of net primary production: Resolving the paradox. *Ecol. Monogr.* **2009**, *79*, 343–377. [[CrossRef](#)]
57. Stoy, P.C.; Richardson, A.D.; Baldocchi, D.D.; Katul, G.G.; Stanovick, J.; Mahecha, M.D.; Reichstein, M.; Detto, M.; Law, B.E.; Wohlfahrt, G.; et al. Biosphere-atmosphere exchange of CO₂ in relation to climate: A cross-biome analysis across multiple time scales. *Biogeosciences* **2009**, *6*, 2297–2312. [[CrossRef](#)]
58. Cuny, H.E.; Rathgeber, C.B.; Frank, D.; Fonti, P.; Makinen, H.; Prislán, P.; Rossi, S.; Del Castillo, E.M.; Campelo, F.; Vavřik, H.; et al. Woody biomass production lags stem-girth increase by over one month in coniferous forests. *Nat. Plants* **2015**, *1*, 15160. [[CrossRef](#)] [[PubMed](#)]
59. Wen, Y.; Jiang, Y.; Jiao, L.; Hou, C.X.; Xu, H. Inconsistent relationships between tree ring width and normalized difference vegetation index in montane evergreen coniferous forests in arid regions. *Trees-Struct. Funct.* **2022**, *36*, 379–391. [[CrossRef](#)]
60. Kagawa, A.; Sugimoto, A.; Yamashita, K.; Abe, H. Temporal photosynthetic carbon isotope signatures revealed in a tree ring through ¹³C₂ pulse-labelling. *Plant Cell Environ.* **2005**, *28*, 906–915. [[CrossRef](#)]
61. Anderegg, W.R.; Schwalm, C.; Biondi, F.; Camarero, J.J.; Koch, G.; Litvak, M.; Ogle, K.; Shaw, J.D.; Shevliakova, E.; Williams, A.P.; et al. Pervasive drought legacies in forest ecosystems and their implications for carbon cycle models. *Science* **2015**, *349*, 528–532. [[CrossRef](#)]

62. Scharnweber, T.; Smiljanic, M.; Cruz-García, R.; Manthey, M.; Wilmking, M. Tree growth at the end of the 21st century—The extreme years 2018/19 as template for future growth conditions. *Environ. Res. Lett.* **2020**, *15*, 074022. [[CrossRef](#)]
63. Skomarkova, M.V.; Vaganov, E.A.; Mund, M.; Knohl, A.; Linke, P.; Boerner, A.; Schulze, E.D. Inter-annual and seasonal variability of radial growth, wood density and carbon isotope ratios in tree rings of beech (*Fagus sylvatica*) growing in Germany and Italy. *Trees* **2006**, *20*, 571–586. [[CrossRef](#)]
64. Richardson, A.D.; Carbone, M.S.; Keenan, T.F.; Czimczik, C.I.; Hollinger, D.Y.; Murakami, P.; Schaberg, P.G.; Xu, X. Seasonal dynamics and age of stemwood nonstructural carbohydrates in temperate forest trees. *New Phytol.* **2013**, *197*, 850–861. [[CrossRef](#)] [[PubMed](#)]
65. Larson, P.R. *The Vascular Cambium: Development and Structure*; Springer Science & Business Media: Berlin, Germany, 2012.
66. Levesque, M.; Andreu-Hayles, L.; Pederson, N. Water availability drives gas exchange and growth of trees in northeastern US, not elevated CO₂ and reduced acid deposition. *Sci. Rep.* **2017**, *7*, 46158. [[CrossRef](#)] [[PubMed](#)]
67. de Soyza, A.G.; Killingbeck, K.T.; Whitford, W.G. Plant water relations and photosynthesis during and after drought in a Chihuahuan desert arroyo. *J. Arid. Environ.* **2004**, *59*, 27–39. [[CrossRef](#)]
68. Liu, H.; Park Williams, A.; Allen, C.D.; Guo, D.; Wu, X.; Anenkhonov, O.A.; Liang, E.; Sandanov, D.V.; Yin, Y.; Qi, Z.; et al. Rapid warming accelerates tree growth decline in semi-arid forests of Inner Asia. *Glob. Chang. Biol.* **2013**, *19*, 2500–2510. [[CrossRef](#)]
69. Williams, A.P.; Allen, C.D.; Macalady, A.K.; Griffin, D.; Woodhouse, C.A.; Meko, D.M.; Swetnam, T.W.; Rauscher, S.A.; Seager, R.; Grissino-Mayer, H.D.; et al. Temperature as a potent driver of regional forest drought stress and tree mortality. *Nat. Clim. Chang.* **2012**, *3*, 292–297. [[CrossRef](#)]
70. Gazol, A.; Ribas, M.; Gutierrez, E.; Camarero, J.J. Aleppo pine forests from across Spain show drought-induced growth decline and partial recovery. *Agric. For. Meteorol.* **2017**, *232*, 186–194. [[CrossRef](#)]
71. Allen, C.D.; Macalady, A.K.; Chenchouni, H.; Bachelet, D.; McDowell, N.; Vennetier, M.; Kitzberger, T.; Rigling, A.; Breshears, D.D.; Hogg, E.H.; et al. A global overview of drought and heat-induced tree mortality reveals emerging climate change risks for forests. *For. Ecol. Manag.* **2010**, *259*, 660–684. [[CrossRef](#)]
72. Chen, L.; Huang, J.G.; Stadt, K.J.; Comeau, P.G.; Zhai, L.H.; Dawson, A.; Alam, S.A. Drought explains variation in the radial growth of white spruce in western Canada. *Agric. For. Meteorol.* **2017**, *233*, 133–142. [[CrossRef](#)]
73. Hogg, E.H.; Michaelian, M.; Hook, T.I.; Undershultz, M.E. Recent climatic drying leads to age-independent growth reductions of white spruce stands in western Canada. *Glob. Chang. Biol.* **2017**, *23*, 5297–5308. [[CrossRef](#)]
74. Worrall, J.J.; Rehfeldt, G.E.; Hamann, A.; Hogg, E.H.; Marchetti, S.B.; Michaelian, M.; Gray, L.K. Recent declines of *Populus tremuloides* in North America linked to climate. *For. Ecol. Manag.* **2013**, *299*, 35–51. [[CrossRef](#)]
75. Badeck, F.W.; Bondeau, A.; Böttcher, K.; Doktor, D.; Lucht, W.; Schaber, J.; Sitch, S. Responses of spring phenology to climate change. *New Phytol.* **2004**, *162*, 295–309. [[CrossRef](#)]
76. Nemani, R.R.; Keeling, C.D.; Hashimoto, H.; Jolly, W.M.; Piper, S.C.; Tucker, C.J.; Myneni, R.B.; Running, S.W. Climate-driven increases in global terrestrial net primary production from 1982 to 1999. *Science* **2003**, *300*, 1560–1563. [[CrossRef](#)] [[PubMed](#)]
77. Piao, S.L.; Wang, X.H.; Park, T.; Chen, C.; Lian, X.; He, Y.; Bjerke, J.W.; Chen, A.P.; Ciais, P.; Tommervik, H.; et al. Characteristics, drivers and feedbacks of global greening. *Nat. Rev. Earth Environ.* **2020**, *1*, 14–27. [[CrossRef](#)]

Disclaimer/Publisher’s Note: The statements, opinions and data contained in all publications are solely those of the individual author(s) and contributor(s) and not of MDPI and/or the editor(s). MDPI and/or the editor(s) disclaim responsibility for any injury to people or property resulting from any ideas, methods, instructions or products referred to in the content.